



Comparison of the Mechanical and Wear-Resistant Properties of WC-13Ni4Cr and WC-10Co4Cr Coatings Obtained by Detonation Spraying

Gao Yang¹ · Gao Chaoqing¹ · Gao Jianyi² · Cai Lin¹

Submitted: 6 August 2018 / in revised form: 27 February 2019 / Published online: 1 April 2019
© ASM International 2019

Abstract The purpose of this study is to investigate the feasibility of replacing cobalt with nickel as a binder in thermal spraying WC-based coatings. Two kinds of coatings WC-13Ni4Cr and WC-10Co4Cr were deposited by the detonation spraying technology in which propane was added into the detonation gases. The relative content of W₂C and W phases in the coatings was calculated by XRD quantitative analysis method. Wear resistance of the coatings was characterized by ASTM G65 rubber-wheel abrasion test. The results indicate that the decomposition of WC particles in both coatings decreases, while the fracture toughness of the coating increases as the propane flow increases. Wear resistance of WC-based coatings is correlated with the hardness and fracture toughness of the coatings. The wear resistance of both coatings is substantially improved when increasing the propane flow rate. Experimental results show that it is feasible to replace cobalt with nickel in thermal-sprayed WC-based coatings.

Keywords decomposition of WC · detonation spraying · fracture toughness · nickel binder · wear resistance

Introduction

Sintered WC-Co hardmetal has been used in cutting tools for nearly one hundred years. Its fracture toughness can reach up to $13 \text{ MPa} \times \text{m}^{1/2}$ which was assessed by the Anstis' formula (Ref 1, 2), and this hardmetal was produced by high-frequency induction heating at $1500 \text{ }^\circ\text{C}$ under a vacuum of 4×10^{-2} torr and pressure of 60 MPa. Such superior mechanical properties are attributed to the sintering process and high solid solubility between cobalt and WC (Ref 2, 3). However, WC-Co may have low corrosion resistance and cobalt is expensive compared to other metals such as nickel. Compared with WC-Co, WC-Ni hardmetal is rarely employed possibly due to low solid solubility between WC and nickel. In addition to WC-Co being used as a hardmetal in cutting tools by the sintering process, it is also widely used in thermal spraying. Usually, the flame temperature in a thermal spraying process (except for cold spraying) is much higher than the melting point of binder metals such as cobalt, resulting in Co binders being melted or partially melted. Moreover, W₂C or even W phase is formed with WC decarbonization and nano-crystalline or amorphous phases may form in the binder with rapid solidification of the melted particles on the substrate (Ref 4-6).

In fact, the mechanical strength of thermal-sprayed WC-Co coatings is much worse than that of sintered WC hardmetal. For example, the fracture toughness of HVOF-sprayed WC-based coatings is only $0.9\text{-}1.5 \text{ MPa} \times \text{m}^{1/2}$ (Ref 7) (assessed by Anstis' formula) which is much lower than that of sintered WC hardmetal. The main reason is the existence of lamellar structure in thermal spray coatings, which leads to cracks propagating between lamellae during indentation fracture toughness experiments, while the

✉ Gao Yang
gaoyang@dlmu.edu.cn

¹ Thermal Spray Center of the Dalian Maritime University, Dalian 116026, People's Republic of China

² Department of Electrical and Computer Engineering, University of California, Davis, Davis, CA, USA

expensive cobalt does not alter the lamellar structure in the coatings.

In view of the characteristics of the thermal spray materials mentioned above, it is of great practical importance to develop materials that can substitute Co binder in WC-based coatings. Considering the solubility between WC and binder phase, as well as the practical application of WC-based coatings in wear and corrosion resistance, research on nickel replacing cobalt as a binder is of practical significance. The structure of nickel is similar to cobalt, and the lattice parameter difference between fcc nickel (0.352 nm) and fcc cobalt (0.354 nm) is very small. Nickel is a promising alternative material to replace cobalt binder because nickel and cobalt have similar properties. Some studies showed that nickel replacing cobalt in WC-based material caused lower hardness (Ref 8), and cobalt-free WC-(W,Cr)₂C-Ni coating had lower fracture toughness than WC-10Co4Cr coating (Ref 9). Studies have been conducted on the substitution of cobalt with Ni or Fe in sintered WC-Co hardmetals (Ref 3). However, as thermal spraying wear-resistant coatings, WC-Co or WC-CoCr coatings with cobalt as the binder are still dominant in industrial applications.

Detonation spraying is one of the most popular methods to prepare WC-based coatings. The performance of detonation-sprayed WC-based coatings depends on process parameters (Ref 10, 11). In detonation spraying processes, oxygen and acetylene are the main gases. In addition, propane is also used for detonation spraying (Ref 12, 13). Compared with acetylene, propane can reduce the temperature of detonation spraying (Ref 14, 15), which may restrain the decarburization of WC. Existing studies on detonation spraying mainly focus on the effect of processing parameters on the decarburization degree of WC (Ref 11, 12). There are also some studies about the influence of binder content on the mechanical properties of HVOF-sprayed WC-Co coatings; it was found that the fracture toughness of coatings increased with the increase in binder content and decreased with the decomposition degree of the WC grains (Ref 5). WC-10Co4Cr coating has been widely used for thermal spraying in corrosion and wear resistance. In our work, a comparison between a known thermal spray coating composition (WC-10Co4Cr) and a new composition (WC-13Ni4Cr) has been conducted. Special attention has been paid to the effect of the binder phase on the decomposition of WC and the wear resistance of the coatings. Meanwhile, in order to advance the in-depth understanding of the fabrication of thermal-sprayed WC-based coatings, it is expected to establish a relationship between the binder and the microstructure and properties of thermal-sprayed WC-based coatings.

Materials and Methods

Deposition of the Coatings

The conventional sintered-crushed WC-13Ni4Cr and WC-10Co4Cr powders were used as feedstock in this study provided by Zigong Carbides Co., Ltd (Zigong, China). The volume fractions of binder phase in WC-13Ni4Cr and WC-10Co4Cr powders are about 27.9 and 23.5%, respectively. As shown in Fig. 1, both powders have the same particle size ranging from 15 to 45 μm . Figure 2 shows the cross-sectional microstructure of both powders. The size of WC grains in WC-13Ni4Cr powder was 0.5–1.5 μm , while the size of WC grains in WC-10Co4Cr powder was 0.2–2 μm . The detonation spray equipment with intermittent powder feeding employed in this study was designed by Dalian Maritime University to prepare WC-based coatings (Ref 16). According to the previous experimental experience (Ref 17), the oxygen and acetylene flow rates were fixed at 49 and 26 standard liter per minute (SLPM), and

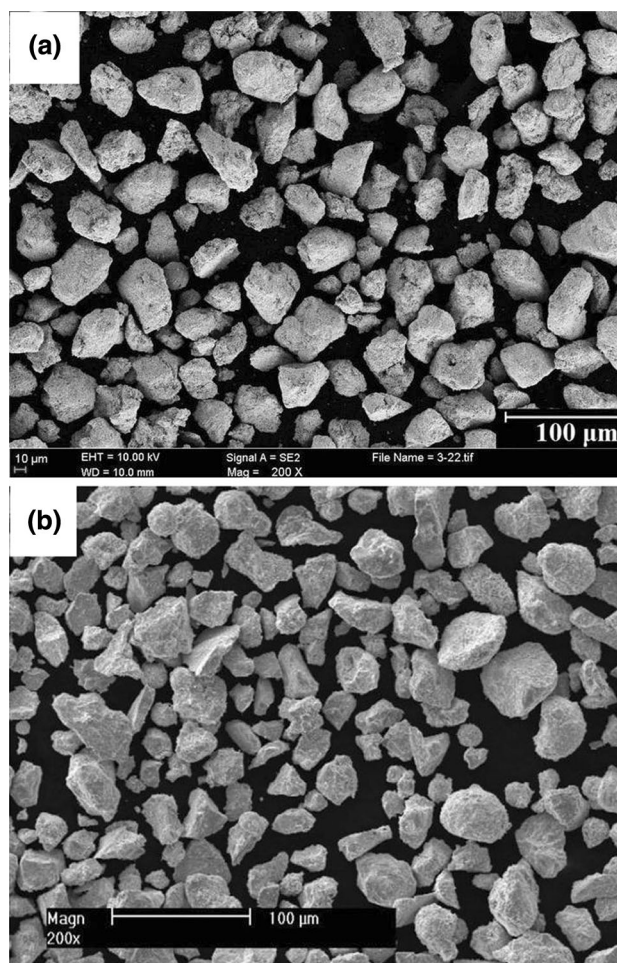


Fig. 1 Morphologies of (a) WC13Ni4Cr and (b) WC10Co4Cr powder, respectively

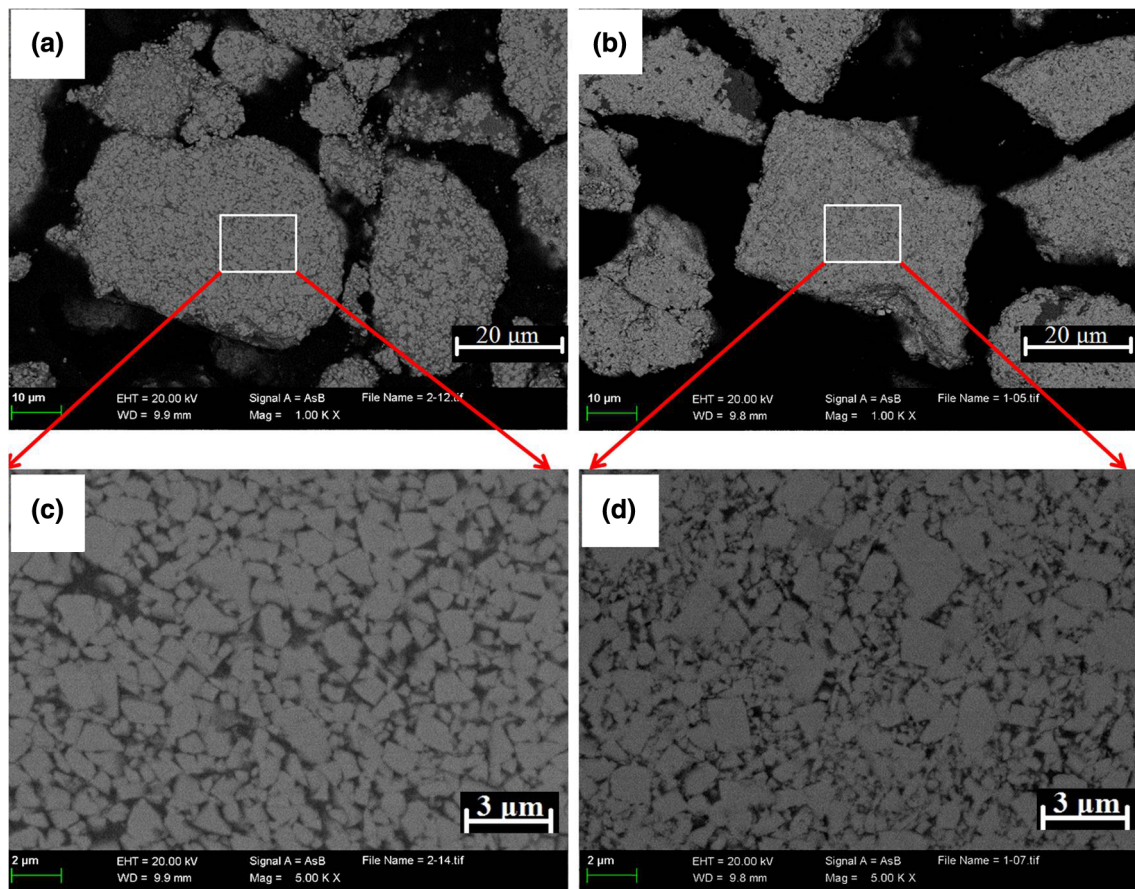


Fig. 2 Cross-sectional morphology of feedstock powders: (a) and (c) WC13Ni4Cr; (b) and (d) WC10Co4Cr

the flow rates of propane gas were chosen as 0, 2, 4, 9 and 14 SLPM, respectively. The processing parameters for coating deposition are listed in Table 1. Stainless steel (316L) cylindrical tubes are used as the substrates. The original external radius and length of the cylindrical substrate are 30.0 and 80.0 mm, respectively. In order to ensure that all substrates have identical external size, substrates were ground by cylindrical diamond grinder. A surface roughness tester (Shanghai Taiming Optical Instrument Co. Ltd., JB-1C) was employed to measure the surface roughness (Ra). Before detonation spraying, substrates were grit-blasted with corundum to get a surface roughness close to 6.2 μm . After coatings deposition, in order to maintain the same surface roughness and size accuracy, the coated specimens were ground by cylindrical diamond grinder again. The Ra of all ground samples for wear resistance testing is about 0.3 μm .

Characterization of the Coatings

The cross-sectional microstructure of the coatings was characterized by field emission scanning electron microscopy (FESEM, Carl Zeiss SUPRATM55) with energy-

Table 1 Detonation spray parameters

Parameters	Values
Oxygen flow rate (SLPM)	49
Acetylene flow rate (SLPM)	26
Propane flow rate (SLPM)	0, 2, 4, 9, 14
Oxygen/fuel ratio, OF	1.9, 1.8, 1.7, 1.4, 1.2
Powder feed rate, g/min	100
Detonation cycles per second	6
Spray distance, mm	155
N ₂ flow rate (SLPM)	20

dispersive spectrometer (EDS). The porosity of the coatings was estimated by a Leco 3001 image analyzer. The phase composition of the powders and coatings was identified by an x-ray diffraction system (Rigaku D/MAX-Ultima, Japan) with Co K α ($\lambda = 0.1790$ nm) radiation. The working voltage and current were 40 kV and 40 mA, respectively. The analyzed scanning range was between 30° and 85° with a step width of 0.02°. The W₂C/WC and W/WC volume ratios were calculated by formulas (1) and (2), respectively (Ref 18, 19).

$$\frac{V_{W_2C}}{V_{WC}} = \frac{I_{W_2C(101)}}{I_{WC(101)}} \times \frac{\left[P_{WC(101)} |F_{hkl}|^2 \left(\frac{1+\cos 2\theta}{\sin^2 \theta \cos \theta} \right) \right]_{WC(101)}}{\left[P_{W_2C(101)} |F_{hkl}|^2 \left(\frac{1+\cos 2\theta}{\sin^2 \theta \cos \theta} \right) \right]_{W_2C(101)}} \quad (\text{Eq 1})$$

$$\frac{V_W}{V_{WC}} = \frac{I_{W(110)}}{I_{WC(101)}} \times \frac{\left[P_{WC(101)} |F_{hkl}|^2 \left(\frac{1+\cos 2\theta}{\sin^2 \theta \cos \theta} \right) \right]_{WC(101)}}{\left[P_{W(110)} |F_{hkl}|^2 \left(\frac{1+\cos 2\theta}{\sin^2 \theta \cos \theta} \right) \right]_{W(110)}} \quad (\text{Eq 2})$$

where P is the multiplicity factor, $P_{WC(101)} = P_{W_2C(101)} = 12$, $P_{W(110)} = 24$. θ is the Bragg angle, and $(1 + \cos 2\theta)/(\sin^2 \theta \cos \theta)$ is the Lorentz-polarization term. The Lorentz-polarization terms of $WC_{(101)}$, $W_2C_{(101)}$ and $W_{(110)}$ are equal to 6.58, 10.35 and 8.27, respectively. I_{hkl} is the peak integral intensity of the peak corresponding to the (hkl) plane of the crystal. $|F_{hkl}|^2$ are the structure factors which can be calculated from Eq 3, which are 31.7, 41.3 and 60.4 for $WC_{(101)}$, $W_2C_{(101)}$ and $W_{(110)}$, respectively.

$$|F(hkl)| = \sum_{j=1}^{j=n} f(j) e^{i2\pi(hx+ky+lz)} \quad (\text{Eq 3})$$

where $f(j)$ is the scattered wave of each atom. x, y, z is the frame of reference, and h, k, l are the Miller indices of the lattice plane.

The Vickers microhardness of the coatings was evaluated on the polished cross-sections with a nominal load of 300 gf and the dwell time of 10 s. For each coating, 15 indentations were made and the mean hardness value was reported. The fracture toughness was measured by an indentation method on the cross-section of coatings at the applied load of 10 kg and the dwell time of 15 s. The indentation fracture toughness was estimated by Eq 4 (Ref 20, 21):

$$K_{IC} = 0.089 \left[\frac{PH_V}{2(c-a)} \right]^{1/2} \quad (\text{Eq 4})$$

P and H_V represent the applied load (N) and Vickers hardness of the coatings, respectively. c and a are the crack length measured from the indentation center to the end of the crack (μm) and half diagonal of the prepared indentation (μm), respectively. Only cracks which are parallel to the substrate starting at the left and the right corners of indents were considered.

The wear resistance of coatings was evaluated by the ASTM G65 dry sand–rubber-wheel (DSRW) abrasion wear test. Dry quartz sand was employed as the abrasive with particle size ranging from 0.2 to 0.6 mm. The flow rate of the quartz sand was 25.0 g/min. The surface speed of the rotating rubber wheel was 96 m/min. During the test, coating specimens were pressed by a normal load of 30 N

against the rubber wheel. The test duration was 30 min. The wear test of each specimen was repeated for 6 times. After wear tests, coating specimens were cleaned with alcohol in an ultrasonic cleaning equipment. Wear mass loss of specimens was measured by an analytical balance.

Results and Discussion

X-ray Diffraction Analysis

X-ray diffraction patterns of both feedstock and coatings obtained at different propane flow rates are shown in Fig. 3. According to the XRD results, it can be found that only the phases of WC and Ni or Co are present in the powders. Note that no $(W,Cr)_2C$ phase was detected in the WC-13Ni4Cr powder, in contrast to a literature (Ref 9) where the $(W,Cr)_2C$ phase was reported in a sintered-

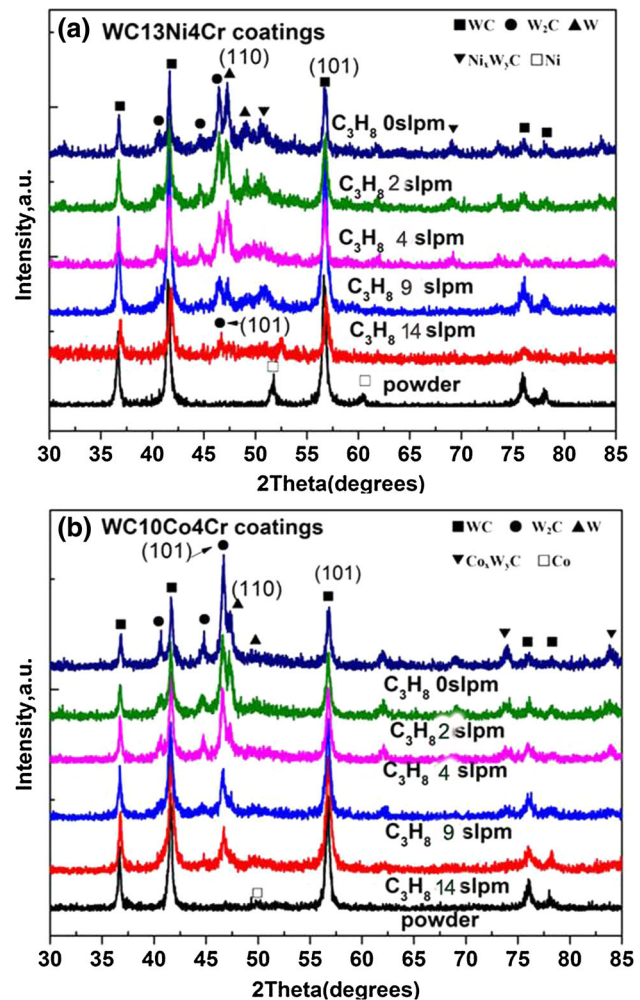


Fig. 3 X-ray diffraction patterns of (a) WC-13Ni4Cr and (b) WC-10Co4Cr powders and its coatings deposited at different propane flows

crushed WC-21Cr₃C₂-6Ni powder and the corresponding HVOF-sprayed coating. To the contrary, W₂C and W phases as well as the η phase of Ni_xW_yC or Co_xW_yC were detected in the WC-13Ni4Cr and WC-10Co4Cr coatings, respectively. The η phase of Co_xW_yC was often found in detonation-sprayed WC-Co and WC-10Co4Cr coatings as reported in previous experiments (Ref 9-12); however, in our experiment the similar Ni_xW_yC phase was also found in detonation-sprayed WC-13Ni4Cr coatings. The Co_xW_yC or Ni_xW_yC phase is stochastically distributed in the coatings, which has a strong relationship with the thermal heating history of the powder in the detonation gases, i.e., it is influenced by the temperature and the oxygen/fuel ratio (OF) of the detonation gases. Although the η phase may have a higher hardness, it is detrimental to the coating fracture toughness because of its inherent brittleness (Ref 11-14). There may have been two causes for the formation of W₂C and W in the thermal-sprayed WC-based coatings. One was that WC loses carbon on its surface which directly reacts with oxygen. The other was that carbon atoms rapidly diffused into the melted binder during the thermal spraying process (Ref 6). As mentioned above, it has been confirmed that the (W,Cr)₂C phase appeared in sintered-crushed WC-21Cr₃C₂-6Ni powder and HVOF-sprayed coating. Bolelli et al. (Ref 9) considered that the diffraction peak of (W,Cr)₂C phase located at $2\theta \approx 39.94^\circ$ slightly shifted from the theoretical peak position of W₂C of $2\theta \approx 39.57^\circ$. Because the diffraction peaks location of W₂C and (W,Cr)₂C are very close, it is difficult to estimate the presence of (W,Cr)₂C phase in the WC-13Ni4Cr coating from current XRD data. In addition, a literature (Ref 22) has shown that the η phase (Co,Cr)₃W₃C or the (Co,Cr,W)₇C₃ phase possibly appears in the HVOF-sprayed WC-10Co4Cr coating. Figure 3 also shows that W₂C, W and η phases in both WC-13Ni4Cr and WC-10Co4Cr coatings gradually reduce and eventually disappear with the increase in the propane flow.

Effect of propane: The formation of W₂C or W is affected dominantly by the oxygen/acetylene ratio (OF) and temperature of WC grains. Babu et al. (Ref 23) found no W phase in the WC-12Co detonation-sprayed coatings at low oxygen/acetylene ratio (OF = 1.16). However, W phase appeared in the coatings when the OF was 1.5. The

content of W phase increased rapidly as the OF raised to 2.0. Based on the literature (Ref 24), the highest combustion temperature of acetylene is 3175 °C at an oxygen/acetylene ratio of 1.4, while the highest combustion temperature of propane is 2840 °C at an oxygen/propane ratio of 4.4. With fixed oxygen/acetylene ratio, the addition of propane will lead to a reduction in the oxygen/fuel ratio of the detonation gas, which can also lead to a decrease in the detonation spraying temperature. In our experiment, the oxygen/fuel ratios (OF) are 1.9, 1.8, 1.7, 1.4 and 1.2 corresponding to propane flow rates of 0, 2, 4, 9 and 14 SLPM.

Effect of the binder: Some literature has reported that the decomposition degree of WC decreased with the increase in Co binder content in HVOF-sprayed WC-Co coatings (Ref 5, 23, 25). The temperature of WC grains decreased with increasing binder phase content during thermal spray, which is due to the specific heat of binder and WC. The data for thermo-physical properties of binder and WC are listed in Table 2 (Ref 5, 26-29). Since the specific heat of cobalt (418.68 J/kg·K) is higher than that of WC (50.2 J/kg·K) at 300-2500 K, the temperature rise of WC grains in the thermal spraying of WC-Co is controlled by the Co content.

The phase volume fraction ratios of W₂C/WC and W/WC in WC-13Ni4Cr and WC-10Co4Cr coatings are illustrated in Fig. 4. The W₂C/WC and W/WC ratios decrease in both coatings with an increase in the C₃H₈ flow rate. The W/WC ratio in the WC-13Ni4Cr coating is obviously higher than that in the WC-10Co4Cr coating when the flow rate of propane is less than 4 SLPM; this phenomenon indicates that nickel binder may cause more severe decomposition of WC than cobalt binder does. As mentioned above, higher binder content should decrease the WC temperature and result in a decrease in the decomposition of WC particles. However, the binder volume fraction (27.9%) in the WC-13Ni4Cr powder is greater than that in the WC-10Co4Cr powder (23.5%) so that the decarburization in the WC-13Ni4Cr coating should be lower than it is in the WC-10Co4Cr coating, but the opposite happened. The reason can be explained as follows: the melting point of nickel (1453 °C) is lower than that of cobalt (1495 °C), which can lead to the decarburization of WC grains in the WC-13Ni4Cr coating easily.

Table 2 Physical properties of binder metal and WC reinforcement phase

Materials	Cobalt	Chromium	Nickel	WC
Thermal conductivity, W/(m K)	96.0	93.7	88.5	197.0
Specific heat, J/(kg K)	418.68	460.548	502.416	50.23
Density, g/cm ³	8.90	7.19	8.91	15.70
Atomic number	27	24	28	...
Melting point, °C	1495	1907	1453	2775
Fusion heat, kJ/mol	15.5	20.9	17.2	...

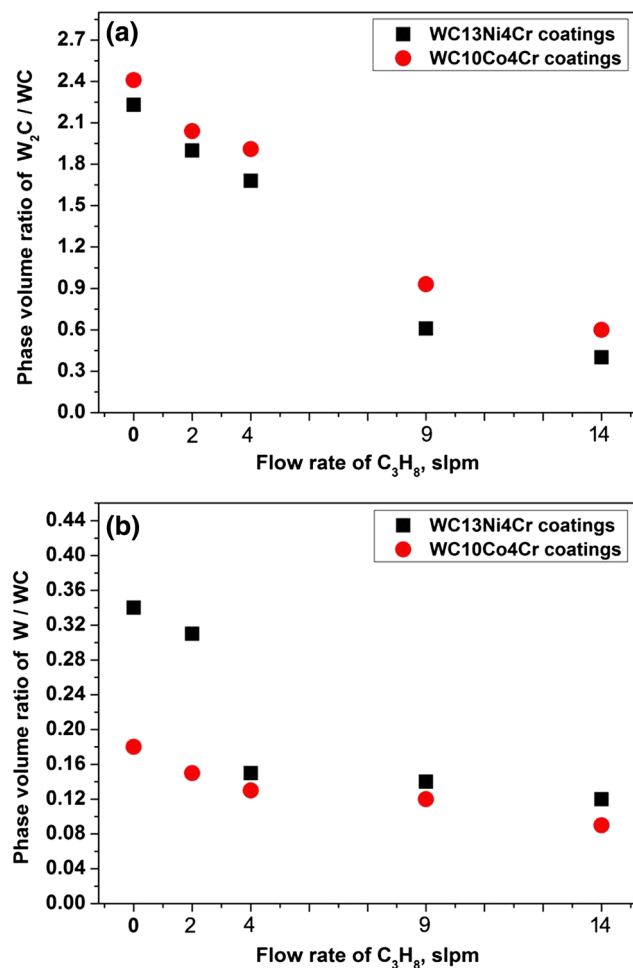


Fig. 4 The phase volume fraction ratios of (a) W_2C/WC and (b) W/WC in WC-13Ni4Cr and WC-10Co4Cr coatings

Moreover, the diffusion coefficients of carbon and tungsten atoms in nickel are higher than they are in cobalt (Ref 30). Furthermore, the WC grain size is 0.5–1.5 μm in WC-13Ni4Cr powder which less than 0.2–2 μm in WC-10Cr4Cr powder. Thus, the decomposition degree of WC in the WC-13Ni4Cr coating is higher than that in WC-10Co4Cr coatings.

Effect of chromium: Besides the effect of nickel and cobalt binders, the influence of chromium should also be considered in both powders and coatings. In the course of actual feedstock powder preparation, it is difficult to prepare several micron grade Co-Cr or Ni-Cr alloy particles. Generally, fine cobalt or nickel powder is used as the metal binder, and then fine chromium carbide powder is added to mix with WC and cobalt or nickel powder. Finally, they were sintered at high temperature to produce WC-10Co4Cr or WC-13Ni4Cr feedstock materials. Some literatures (Ref 9, 31–34) have indicated that Cr_3C_2 is not stable at 1250 °C in the 70%WC-24% Cr_3C_2 -6%Ni mixture. The reaction between WC and Cr_3C_2 was observed, resulting in the

formation of a small amount of $(W,Cr)_2C$ phase a powder with a Cr_3C_2 content as high as 24 wt.%. However, the $(W,Cr)_2C$ phase was not detected in either WC-13Ni4Cr powder or coating in our experimental results. The reason may be that the amount of Cr_3C_2 added to the powder is small, which is difficult to be detected by XRD. On the other hand, Bolelli et al. (Ref 22) reported $(W,Cr)_2C$ phase formation for the WC-10Co4Cr powder. $(Co,Cr,W)_7C_3$ carbides can be formed above the solubility limit of chromium in the binder at high carbon content. However, η -phase may be formed when carbon content is below the nominal carbon content. Therefore, the added chromium carbide is unlikely to exist in the form of metallic chromium binder but is more likely to react with WC to form a $(W,Cr)_2C$ compound in WC-13Ni4Cr powder and $(Co,Cr,W)_7C_3$ carbides or η -phase in the WC-10Co4Cr powder. They were difficult to be detected by XRD since the location of diffraction peaks of $(Co,Cr,W)_7C_3$ and Cr_3C_2 phases are very closed to those of fcc.-Co or η -phase.

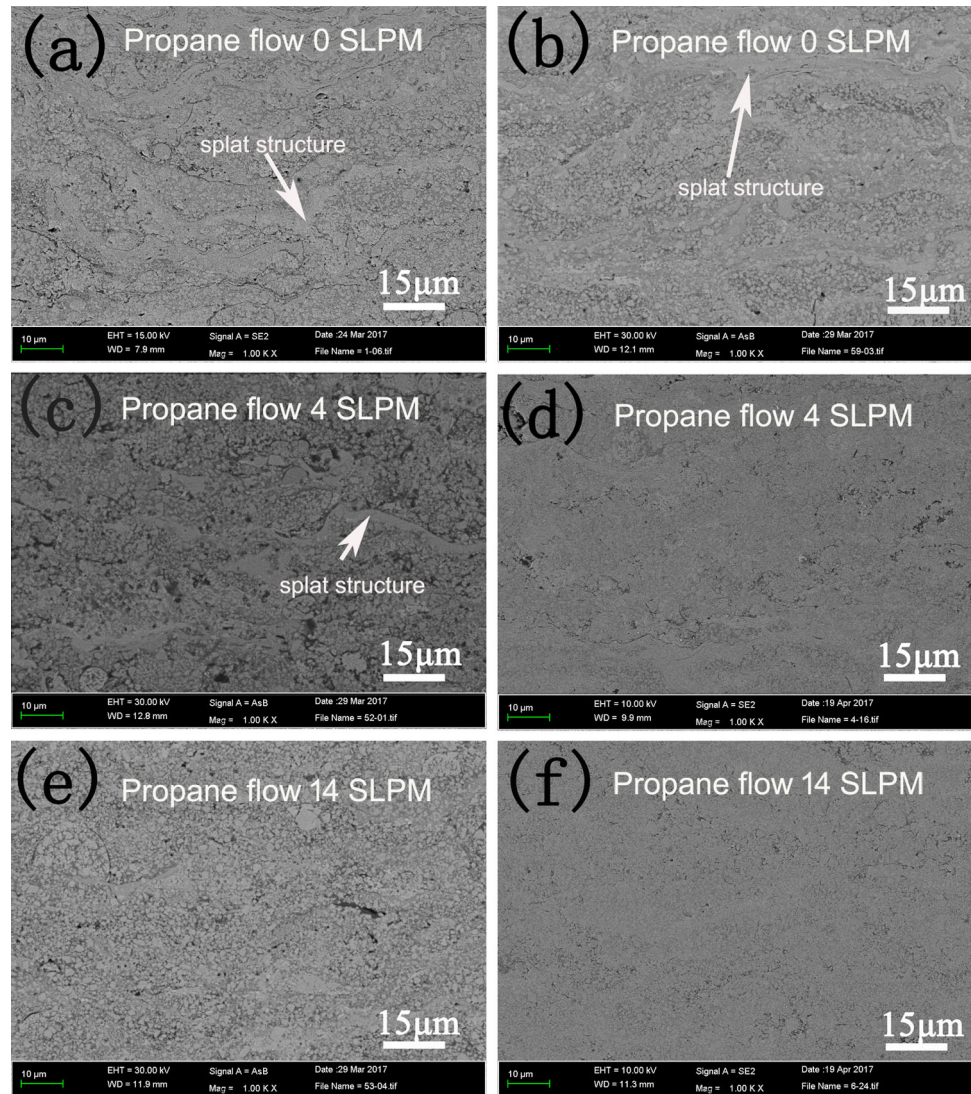
Microstructure Characterization

Figure 5 and 6 shows the cross-sectional microstructure of the coatings as a function of the propane gas flow with low and high magnification. The typical structure of WC grains and “splat structure” was found in the WC-10Co4Cr and WC-13Ni4Cr coatings. The composition of each region in the coatings was analyzed by EDS and results are shown in Table 3. W, Co, Cr, C in the splat structure (region B) and Co, Cr in the binder region (region A) were detected for WC-10Co-4Cr coatings. Furthermore, Cr was not detected in WC grains. W, Ni, Cr, C in the “splat structure” and Ni, Cr in the binder region were detected for WC-13Ni4Cr coatings. Cr was also detected in WC grains for WC-13Ni4Cr coatings as opposed to the WC-10Co-4Cr coating. Note that the influence of surrounding element is ineluctable since the area of the binder region is very small. According to the EDS analysis and XRD data, we conclude that the splat structure in the WC-13Ni4Cr and WC-10Co-4Cr coatings may be Ni_xW_yC and Co_xW_yC or $Ni_xW_yCr_zC$ and $Co_xW_yCr_zC$, respectively.

Hardness and Fracture Toughness

The hardness of the two types of coatings as a function of propane flow rates is shown in Fig. 7. The hardness of the WC-13Ni4Cr coating gradually increased with the increase in the propane flow rate from 0 to 4 SLPM and then remained unchanged. This phenomenon may be attributed to higher W/WC ratio in the WC-13Ni4Cr coating in the low propane range from 0 to 4 SLPM. Namely, the hardness of the WC-13Ni4Cr coating increased gradually with

Fig. 5 Cross-sectional microstructure of the coatings: (a), (c) and (e) WC13Ni4Cr, and (b), (d) and (f) WC10Co4Cr coatings deposited at flow rates of propane 0, 4 and 14 SLPM, respectively



increasing propane flow rate, since the W/WC ratio correspondingly decreased in the WC-13Ni4Cr coating. On the other hand, the hardness of the WC-10Co4Cr coating remained almost unchanged or slightly decreased in the range of propane flow from 0 to 14 SLPM. This phenomenon may be attributed to the phase change in the WC-10Co4Cr coating. Increasing OF ratio promotes the formation of W_2C or η phase, which may lead to a slight increase in the hardness of the coating. When the flow rate of C_3H_8 is zero, the hardness of the WC-13Ni4Cr coating is about 200 kg/mm^2 lower than that of the WC-10Co4Cr coating. This phenomenon may be attributed to high W/WC ratio and high binder content in the WC-13Ni4Cr coating. The difference in hardness of both coatings gradually decreased with the increase in the propane flow rate and became negligible when the flow rate of C_3H_8

reached 9 SLPM. This is due to the decrease in decarburization of the two coatings as the propane flow rate increased.

The fracture toughness of the coatings as a function of propane flow is shown in Fig. 8. The fracture toughness of the WC-13Ni4Cr coating was lower than that of the WC-10Co4Cr coating when the propane flow was 0, 2, 4 SLPM, respectively. However, when the propane flow was 9 and 14 SLPM, the fracture toughness values of the WC-13Ni4Cr and WC-10Co4Cr coatings were comparable. The fracture toughness of the coatings not only increases with their hardness, but is also sensitive to the phases in the coating (Ref 32–34). By increasing the degree of WC decomposition, the content of W_2C or η phase increased in the coating and fracture toughness of the coatings decreased.

Fig. 6 Cross-sectional microstructure of the coatings: (a), (c) and (e) WC13Ni4Cr, and (b), (d) and (f) WC10Co4Cr coatings deposited at flow rates of propane 0, 4 and 14 SLPM, respectively

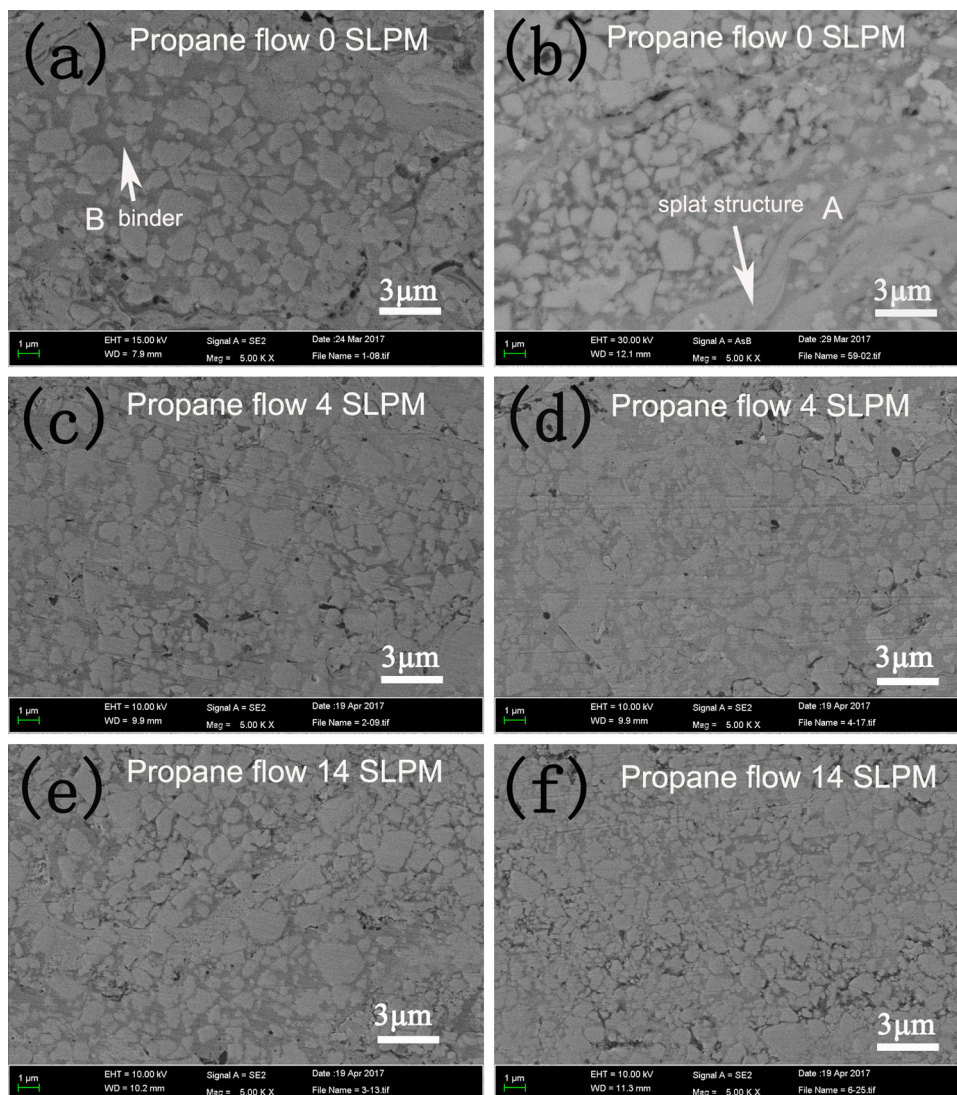


Table 3 The composition of the binder and splat structure by EDS analysis in at.%

Coatings-propane flow	Binder				Splat structure			
	W	Ni or Co	Cr	C	W	Ni or Co	Cr	C
WC-13Ni4Cr-0	24.83	14.15	1.82	59.2	24.52	19.38	1.98	54.12
WC-13Ni4Cr-4	9.35	26.73	3.29	60				
WC-13Ni4Cr-14	10.07	27.77	3.09	59				
WC-10Co4Cr-0	18.96	3.36	3.0	74	15.64	7.17	1.86	60
WC-10Co4Cr-4	21.57	13.55	5.24	59				
WC-10Co4Cr-14	16.15	12.16	3.63	68				

Wear Resistance

Two sets of coatings deposited at propane flow rates of 0, 4, and 14 SLPM were selected to carry out the abrasive wear tests. The weight loss of the coatings with a wear time of 30 min is shown in Fig. 9. The relationship between wear time and weight loss without propane is shown in

Fig. 10. The abrasion loss increases almost linearly with the wear time for both coatings, and the weight loss of the WC-13Ni4Cr coating is remarkably higher than that of the WC-10Co4Cr coating when the propane flow rate is zero. This result may correspond to higher W/WC phase in the WC-13Ni4Cr coating which results in the lower fracture toughness as well as lower hardness of this coating in

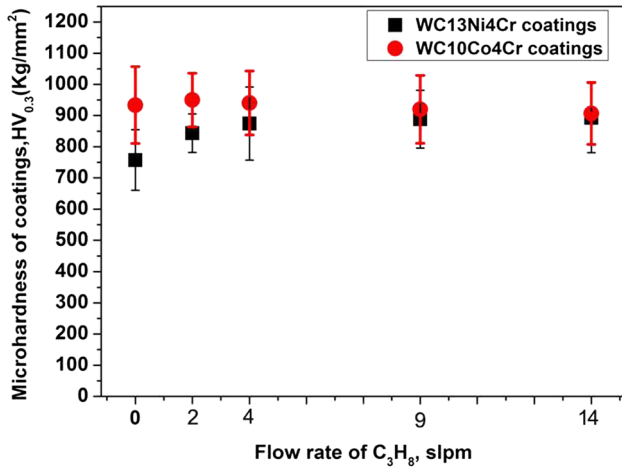


Fig. 7 The hardness of the WC-13Ni4Cr and WC-10Co4Cr coatings as a function of propane flow rate

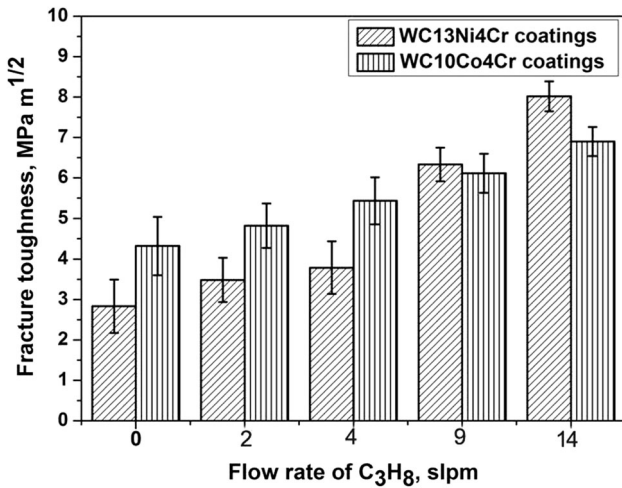


Fig. 8 The fracture toughness of the WC-13Ni4Cr and WC-10Co4Cr coatings as a function of propane flow rates

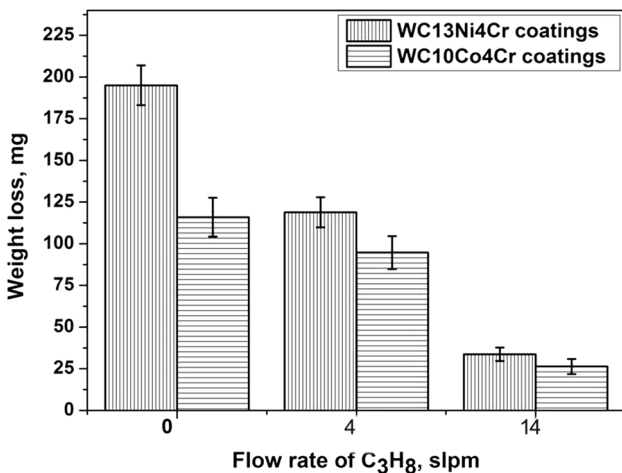


Fig. 9 The weight loss of the coatings deposited at propane flow rate of 0, 4, 14 SLPM and with a wear time of 30 min

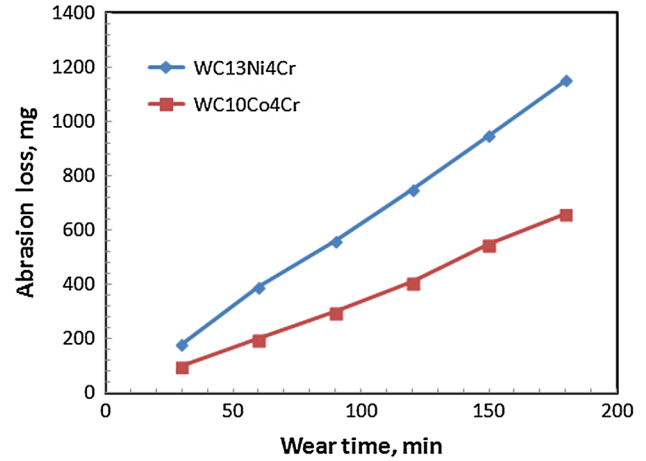


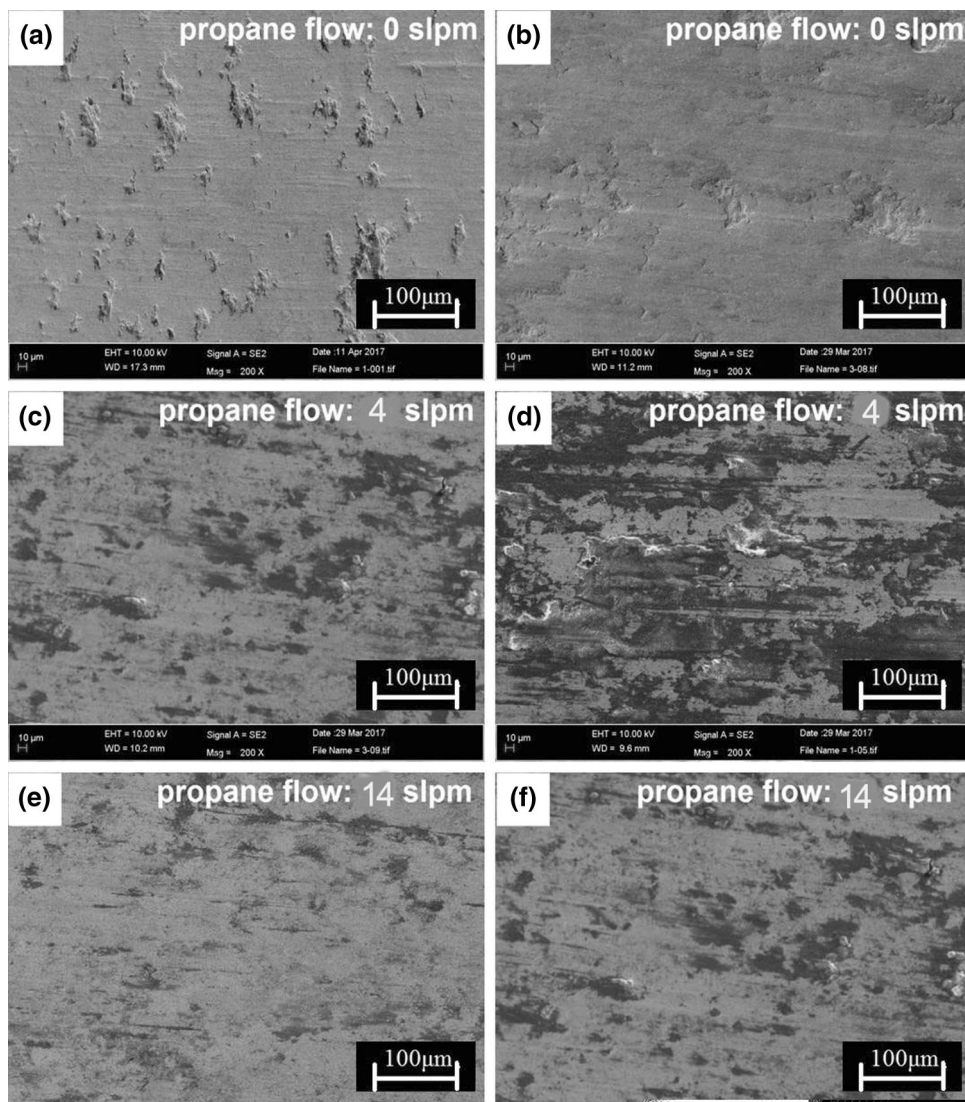
Fig. 10 The relationship between wear time and weight loss for WC-13Ni4Cr and WC-10Co4Cr coatings without propane added

comparison with the WC-10Co4Cr coating. When the propane flow rate was 4 SLPM, the weight loss of the WC-13Ni4Cr coating was still higher than that of the WC-10Co4Cr coating, while the difference was significantly reduced. The wear weight loss of the WC-13Ni4Cr and WC-10Co4Cr coatings was almost the same when the propane flow rate was 14 SLPM. It may be attributed to the increase in fracture toughness of both coatings and to their nearly identical hardness values with the increase in propane flow rate. Higher fracture toughness coating resulted in higher wear resistance under the same hardness value. Overall, the wear resistance of the two types of coatings was substantially improved with the increase in the fracture toughness. Many literature sources (Ref 35-37) have reported that the wear resistance of the coatings is related to their fracture toughness, especially dominated by the loss of ductility in the Co-rich binder phase due to its amorphization.

The worn surface morphology of coatings at a wear distance of 3 km observed by field emission scanning electron microscopy is shown in Fig. 11. In the case without propane, many “brittle crackings” can be found on the worn surface of the coatings, especially the density of the brittle crackings on the worn surface of the WC-13Ni4Cr coatings is higher than that on the worn surface of the WC-10Co4Cr coatings (Fig. 11a and b), which implies that the “brittle cracking” is a main phenomenon during the abrasive wear process, and it is due to the lower fracture toughness. The increase in propane flow rate resulted in an increase in the fracture toughness which resulted in the reduction of “brittle cracking.” The “abrasive grooving” became the main pattern (Fig. 11c and d).

The wear resistances of the WC-13Ni4Cr and WC-10Co4Cr coatings were improved with the increase in fracture toughness despite the different binders. The results of the present study suggest that nickel binder is a good

Fig. 11 The worn surface morphology of the coatings after a wear time of 30 min, observed by field emission scanning electron microscopy. (a), (c) and (e) WC-10Co4Cr coatings and (b), (d) and (f) WC-13Ni4Cr coatings deposited with propane flow rates of 0, 4 and 14 SLPM, respectively



replacement of cobalt in detonation-sprayed WC-based coatings when the propane flow rate equals 14 SLPM. Substantially improved wear resistance of WC-Ni coatings may accelerate the research progress and industrial application of the replacement of precious cobalt with cheap nickel in WC-based coatings.

Conclusions

In the detonation spraying process, the addition of a suitable amount of propane into the oxygen–acetylene detonation gas mixture reduced the oxygen/fuel ratio and the flame temperature, which leads to decreased decomposition of WC particles. The wear resistance of WC-based coatings was correspondingly improved. At low propane flow rate, WC decomposition level in the WC-13Ni4Cr coating was higher than that in the WC-10Co4Cr coating. The content

of W phase in the WC-13Ni4Cr coating was relatively high. With the increase in the propane flow rate, WC decomposition in both coatings substantially decreased and fracture toughness of the coatings was gradually improved. The wear resistance of the WC-10Co4Cr coating was better than that of the WC-13Ni4Cr coating at low propane flow rate. However, the wear resistance discrepancy between the two kinds of coatings was gradually reduced, indicating the potential of replacing cobalt with a nickel binder in thermal-sprayed WC-based coatings, and the wear resistance of coatings was improved with the increase in the propane flow rate. The decomposition degree of WC grains had a significant influence on microstructure, fracture toughness and wear resistance of WC-based coatings. When the decomposition degree of WC grains was controlled at a low level, wear pattern changed from brittle cracking to abrasive grooving with increasing fracture toughness of the coating.

References

- G.R. Anstis, P. Chantikul, B.R. Lawn, and D.B. Marshall, Indentation Techniques for Measuring Toughness of Ceramics, *J. Am. Ceram. Soc.*, 1981, **64**, p 533
- H.C. Kim, I.J. Shon, J.K. Yoon, and J.M. Doh, Comparison of Sintering Behavior and Mechanical Properties Between WC-8Co and WC-8Ni Hard Materials Produced by High-Frequency Induction Heating Sintering, *Met. Mater. Int.*, 2006, **12**, p 141-146
- F. Klocke, Manufacturing Processes, in: *Cutting Tool Materials and Tools*, 2011 ed. (Springer, Berlin, 2011), pp. 126-133.
- A.H. Dent, S. Depalo, and S. Sampath, Examination of the Wear Properties of HVOF Sprayed Nanostructured and Conventional WC-Co Cermets with Different Binder Phase Contents, *J. Therm. Spray Technol.*, 2002, **11**, p 551-558
- P. Chivavibul, M. Watanabe, S. Kuroda, and K. Shinoda, Effects of Carbide Size and Co Content on the Microstructure and Mechanical Properties of HVOF-Sprayed WC-Co Coatings, *Surf. Coat. Technol.*, 2007, **202**, p 509-521
- C. Verdon, A. Karimi, and J.-L. Martin, A Study of High Velocity Oxy-Fuel Thermally Sprayed Tungsten Carbide Based Coatings Part I: Microstructures, *Mater. Sci. Eng.*, 1998, **A246**, p 11-24
- P. Chivavibul, M. Watanabe, and S. Kuroda, Effect of Microstructure of HVOF Sprayed WC-Co Coatings on Their Mechanical Properties, in *Thermal Spray 2007: Global Coating Solutions, on CD-ROM*, ed. by B.R. Marple, M.M. Hyland, Y.-C. Lau, C.-J. Li, R.S. Lima, and G. Montavon (ASM International, Beijing, 2007), p. 1212.
- V.A. Tracey, Nickel in Hardmetals, *Int. J. Refract. Met. Hard Mater.*, 1992, **11**, p 137-139
- G. Bolelli, L.-M. Berger, M. Bonetti, and L. Lusvarghi, Comparative Study of the Dry Sliding Wear Behavior of HVOF-Sprayed WC-(W, Cr)2C-Ni and WC-CoCr Hardmetal Coatings, *Wear*, 2014, **309**, p 96-111
- R.C. Tucker, Plasma Spray, Detonation Gun, and HVOF Deposition Techniques, *Materials and Processes for Surface and Interface Engineering*, Y. Pauleau, Ed., Praxair S.T. Technology, Inc., Danbury, 1995, p 245-284
- P. Suresh Babu, B. Basu, and G. Sundararajan, Processing-Structure-Property Correlation and Decarburization Phenomenon in Detonation Sprayed WC-12Co Coatings, *Acta Mater.*, 2008, **56**, p 5012-5026
- H. Du, W.G. Hua, J.G. Liu, J. Gong, C. Sun, and L.S. Wen, Influence of Process Variables on the Qualities of Detonation Gun Sprayed WC-Co Coatings, *Mater. Sci. Eng. A*, 2005, **408**, p 202-210
- Q. Wang, J. Xiang, G.Y. Chen, Y.L. Cheng, X.Q. Zhao, and S.Q. Zhang, Propylene Flow, Microstructure and Performance of WC-12Co Coatings Using a Gas-Fuel HVOF Spray Process, *J. Mater. Process. Technol.*, 2013, **213**, p 1653-1660
- G. Sundararajan, D. Sen, and G. Sivakumar, The Tribological Behavior of Detonation Sprayed Coatings: The Importance of Coating Process Parameters, *Wear*, 2005, **258**, p 377-391
- V. Ulianitsky, I. Batraev, D. Dudina, and I. Smurov, Enhancing the Properties of WC/Co Detonation Coatings Using Two-Component Fuels, *Surf. Coat. Technol.*, 2017, **318**, p 244-249
- Y. Gao, *A Set of Intermittent Detonation Sprayed Equipment* (China, 2008), Patent ZL 200810076407.7.
- Y. Gao, Z. Hei, X. Xu, and G. Xing, Formation of Molybdenum Boride Cermet Coating by the Detonation Spray Process, *J. Therm. Spray Technol.*, 2001, **10**, p 456-461
- Y. Zhou and G.H. Wu, *Analysis Methods in Materials Science X-ray Diffraction and Electron Microscopy in Materials Science*, 2nd ed., Harbin Institute of Technology Press, Harbin, 2007
- D. Gu, *Laser Additive Manufacturing of High Performance Materials*, Springer, Berlin, 2015
- D.K. Shetty, I.G. Wright, and P.N. Mincer, Indentation Fracture of WC-Co Cermets, *J. Mater. Sci.*, 1985, **20**, p 1873-1882
- J.M. Guilemany, J.M. de Paco, J. Nutting, and J.R. Miguel, Characterization of the W₂C Phase Formed During the HVOF Spraying of WC-12Co Powder, *Metall. Mater. Trans. A*, 1999, **30**, p 1913-1921
- G. Bolelli, L.-M. Berger, T. Börne, H. Koivuluoto, L. Lusvarghi, C. Lyphout, N. Markocsan, V. Matikainen, P. Nylén, P. Sasatelli, R. Trache, and P. Vuoristo, Tribology of HVOF- and HVOF-Sprayed WC-10Co4Cr Hardmetal Coatings: A Comparative Assessment, *Surf. Coat. Technol.*, 2015, **265**, p 125-144
- P. Suresh Babu, B. Basu, and G. Sundararajan, A Comparison of Mechanical and Tribological Behavior of Nano-structured and Conventional WC-12Co Detonation Sprayed Coatings, *J. Therm. Spray Technol.*, 2013, **22**, p 478-490
- W. Krömmner and P. Heinrich, München, Selective Impact of Industrial Gases on the Thermal Spray Process, in *Thermal Spray: Global Solutions for Future Application, International Thermal Spray Conference & Exposition* (DVS Media GmbH, Düsseldorf, 2010), pp. 243-246.
- J.A. Picas, E. Rupérez, M. Punset, and A. Forn, Influence of HVOF Spraying Parameters on the Corrosion Resistance of WC-CoCr Coatings in Strong Acidic Environment, *Surf. Coat. Technol.*, 2013, **225**, p 47-57
- F. Habashi, *Handbook of Extractive Metallurgy II*, Wiley, Heidelberg, 1997
- C.J. Smithells, *Smithells Metals Reference Book*, Butterworths, London, 1983
- G.V. Samsonov, *Handbooks of High-Temperature Materials Properties Index*, Plenum Press, New York, 1964
- Y.H. Xiong, W.H. Hofmeister, Z. Cheng, J.E. Smugeresky, E.J. Lavernia, and J.M. Schoenung, In Situ Thermal Imaging and Three-Dimensional Finite Element Modeling of Tungsten Carbide-Cobalt During Laser Deposition, *Acta Mater.*, 2007, **57**, p 5419-5429
- J.G. Yang, H.B. Wang, Y. Liu, and B.Y. Huang, Diffusion Coefficient of C in Co Binder Phase, *Mater. Sci. Eng. Powder Metall.*, 2007, **12**, p 82-86
- A.A. Bondar, V.A. Maslyuk, T.Ya. Velikanova, and A.V. Grytsiv, Phase Equilibria in the Cr-Ni-C System and Their Use for Developing Physicochemical Principles for Design of Hard Alloys Based on Chromium Carbide, *Powder Metall. Met. Ceram.*, 1997, **36**(5-6), p 242-252
- B.H. Kear, G. Skandan, and R.K. Sadangi, Factors Controlling Decarburization in HVOF Sprayed Nano-WC/Co Hardcoatings, *Scr. Mater.*, 2001, **44**, p 1703-1707
- Š. Houdková and M. Kašparová, Experimental Study of Indentation Fracture Toughness in HVOF Sprayed Hardmetal Coatings, *Eng. Fract. Mech.*, 2013, **110**, p 468-476
- J. Yuan, Q. Zhan, J. Huang, S. Ding, and H. Li, Decarburization Mechanisms of WC-Co During Thermal Spraying: Insights from Controlled Carbon Loss and Microstructure Characterization, *Mater. Chem. Phys.*, 2013, **142**, p 165-171
- D.A. Stewart, P.H. Shipway, and D.G. McCartney, Abrasive Wear Behavior of Conventional and Nano-composite HVOF-Sprayed WC-Co Coatings, *Wear*, 1999, **225**, p 789-798
- Y. Qiao, T.E. Fischer, and A. Dent, The Effects of Fuel Chemistry and Feedstock Powder Structure on the Mechanical and Tribological Properties of HVOF Thermal Sprayed WC-Co Coatings with Very Fines Structures, *Surf. Coat. Technol.*, 2003, **172**, p 24-41
- A.C. Bozzi and J.D.B. Mello, Wear Resistance and Wear Mechanisms of WC-12Co Thermal Sprayed Coatings in Three-Body Abrasion, *Wear*, 1999, **233**, p 575-587

Publisher's Note Springer Nature remains neutral with regard to jurisdictional claims in published maps and institutional affiliations.